Response to the Reviewer # 1 comments.

We would like to thank the Reviewer for his positive evaluation of the paper, constructive comments and careful paper reading. Technical issues were addressed directly in the revised version of the manuscript. Below are our answers to the main points raised by the Reviewer:

"How much effort is it to obtain the velocity vectors for an individual image pair? If it is a lot of work: Can you share the software code such that researchers can run it for their own individual time/location of interest? If it is not much work: Can you make this method operational and provide to others the velocity vectors at all times/locations where appropriate image pairs from Sentinel 1A/B exist?"

In general, our data processing scheme includes two separate tasks – data pre-processing and velocity calculation. The first step includes cutting out the overlapping SAR image fragments, their calibration and normalization, and is planned to be automated soon. The second step (velocity calculation) also needs some additional work with image fragments prior to velocity calculations (e.g. data filtering) and during post-processing (e.g. elimination of false correlations), and currently is done in supervised manner. These two steps are made separately and not yet combined into a single code/procedure. We are working now toward the automatization of the entire procedure to provide velocity vectors to all interested users at least over a single pre-selected site (e.g. Fram Strait), as suggested by the reviewer. Yet, there are still many small issues of the processing chain that are subject of constant improvement, but we hope to finish it asap, at least in the simplified way using the MCC method at the core.

"When can this method be used? What is the range of sea ice concentrations where it applies? Are there differences between seasons in the detail/precision/ease with which the method can be used? E.g. maybe in July (melt season) there is less texture on the sea ice that the satellite could pick up than in September (start of refreezing). Are there influences of weather on the method (e.g. clouds, fog)?"

We haven't yet tested the method over a very large number of paired SAR images spanning different seasons, background ice concentrations and other environmental factors (like near-surface winds), but our experience from various dates in summer season of 2017 suggests that the MCC works rather effectively for typical sea ice concentrations encountered in the marginal ice zone (20-80%), provided the movement of ice floes is apparent in the sequential SAR images. Though our current experience is lacking to address the question regarding the season, we already plan a more detailed study spanning a longer period of SAR observations over the Fram Strait MIZ.
The major issue arising during the processing is the change in the SAR viewing geometry between two sequential scenes. Usually, the desired region of interest would be seen in the near-range in one image, and in the far-range in another. As a result, the level of radar backscatter (signal strength) over the particular surface area would be different, and so would affect the clarity of eddy manifestation in each of the SAR images in the pair. In such case, individual ice floes shaping the eddy structure might be well seen in one image and poorly seen or have inverted radar contrast in the another one. This issue is addressed during the normalization step, but might be difficult to overcome for very thin ice (either in the beginning of melt season or during freeze onset) whose radar backscatter might become inverted due to the differences in the viewing geometry or varying winds.
In regard to weather conditions, SAR is not sensitive to fog and clouds as microwaves effectively penetrate through the atmosphere. Yet, the locally varying near-surface winds may cause some difficulties in the data analysis as described above. If the near-surface winds change over the region of interest during existing time gap between sequential observations, this again might change the radar contrast (signal level) of the sea ice features traced in MCC, resulting e.g. in low correlations and/or inability to retrieve horizontal currents over such ice-covered pixels.
Condensed answer to the above two questions is now introduced in the paper.

The example presented here is from September 2017 in the marginal ice zone in Fram Strait. My high resolution shipboard in-situ study of a submesoscale filament (von Appen et al GRL 2018) was from July 2017, i.e. 3 months earlier. Is there a reason you chose the later time? A direct comparison between the in-situ and the remote sensed data could benefit both methods and reveal more

information on the ocean than to consider them separately. I'm not suggesting to change the example presented here, but it might be nice to follow up by also using the method on the July 2017 example, hence also the motivation for the questions under point 1 above.

The only reason here was to show the applicability of the method to retrieve both meso- and submesoscale dynamics in the MIZ. That is why we have chosen specifically the SAR data from 17 September, when the development of the large anticyclone was observed in the MIZ, out of many other paired images in September 2017 (and other months, including July 2017). We completely agree with the reviewer and would be happy to make a follow-on study considering the entire summer season including the dates when the high-resolution cruise measurements were made in July 2017.

'The grammar in the manuscript needs careful editing. Especially articles (a/the) are often missing. I point out a few (but by no means all) of these instances below. I'm not sure whether this should be done now or will take place anyways after acceptance by the journal's copy editors.

Thank you for pointing the grammar issues of the text, we have tried to do our best to improve it.

l23 Can that melt rate also be expressed as m/day in the vertical?

Here we simply cite the facts that are given in the original paper by Johannessen et al. (1987) in the form that emphasizes the horizontal melt rates. As we do not address vertical melt rates further in the paper, the present form seems to be acceptable. However, if the Reviewer insists we can make that change.

l39 Can you give a number what "relatively low concentrations" means (see main point 1 above)?

In this part of text we cite the paper by Manucharyan and Thompson (2017), where sea ice concentrations considered were from 50% down to zero. This is now included in the text.

l88 "the velocity detection threshold in this case would be 0.03 m s-1" I think it is not just the threshold, but also the precision of your method. I.e. you can only determine the velocity to be 0.03m/s, 0.06m/s, 0.09m/s, and so on. Or am I misunderstanding this?

In fact, this '0.03 m s-1' is the lower limit below which we can't resolve the object's movement working with S-1 GRD EW mode images. The precision of velocity calculations is then set up by the pixel spacing (equal to 40 m) which equals to 40 m/48 min = $\pm$ 0.01 m s^{-1}. This is now added to the text.

l93 Did you mean 1150km^2? Otherwise the area would only be 2km long (multiplied by 60 km width).

Thank you for noting this typo, the correct value is ~ 15 000 km^2 as the average length of the MIZ was about 220 km long (being 60 km iwde).

"meaning" How does the second statement (reflects underlying circulation) follow from the first statement (3-5m/s)? Maybe you should state that the winds were very weak or something like that.

Thank you, we have slightly rephrased this sentence. Now it sounds:
"According to WindSat and ASCAT scatterometers' data for 17 September 2017 (not shown), the wind conditions were characterized by low south-easterly winds of 3-5 m s^{-1} under which the ice drift near the ice edge should reflect the underlying ocean circulation (Shuchman et al., 1987; Manucharyan and Thompson, 2017)."

l165 "instability, of"

Here we meant "the barotropic and baroclinic instability of an ice edge jet…". Shall it be separated by comma in this case?

Fig3 Consider to also show strain in a subplot. Also add the "A, C1, F1" letters and the F1 arrows to all subplots to make a comparison easier.

Thank you for the suggestion. In fact, we are already at the limit of the word count and paper length for the manuscript type "Brief Communication". We, therefore, have no extra space to accommodate one more subplot and its description in the text. This can only be done at the expense of other material in the paper.

Response to the Reviewer # 2 comments:

We would like to thank the Reviewer for his positive evaluation of the paper, constructive comments and helping us to improve the quality of the text by specifying many text edits that were fixed directly in the revised version of the manuscript. Below are our answers to the main points raised by the Reviewer:

"The paper title should preferably be modified to read: Mesoscale and submesoscale dynamics in the marginal ice zone from sequential SAR observations. The abstract is perhaps too brief. The importance for model validation should be mentioned in consistence with the Discussion and conclusion section."

Thank you for the comments. According to the Cryosphere journal rules, all short papers must be entitled starting with "Brief Communication: …". We completely agree with changing of 'of the MIZ' to 'in the MIZ'. Regarding the abstract length, it was made according to the journal rules for such paper types when the abstract is limited by 100 words only. These rules are specified at the journal homepage at https://www.the-cryosphere.net/about/manuscript_types.html. Nevertheless, we have managed to mention the 'model validation' in the abstract which now counts for 97 words.

"The submesoscale dynamics are also recognized to have intense, narrow bands of vertical motion. The authors need to address this issue in regard to the application of the MCC method whereby only the estimation of horizontal motion is discussed. For instance, could patterns evolve as influenced by the vertical motion, rather than the horizontal motion. The marginal ice zone is periodically also known to have bands of strong wind induced upwelling that would also influence the subsequent dynamics."

Thank you for this important point. We agree that intense vertical motions associated with submesoscale dynamics may impact the evolution of sea ice patterns observed in the SAR images. This might either be due to upwelling of relatively warm subsurface water to the ocean-ice interface in the narrow surface current divergence zones resulting in gradual sea ice melt at the surface, or the surface water subduction in the current convergence zones that was well described e.g. by von Appen et al. (2018) in the study region from in situ sampling. In fact, this is something we have briefly mentioned in the introduction and addressed in more details when showing the horizontal divergence field in Fig. 3b. The latter clearly shows the formation of intense surface current convergence/divergence zones where sea ice accumulates/repel and the surface water goes down/up. In this sense, surface current retrieval using the MCC not only shows the regions of intense horizontal currents, but also the surface areas with intense vertical motions marked by high surface current divergence/convergence values. On the another hand, we might expect that the time interval between sequential SAR acquisitions (around 1 hour) is perhaps too short to see the direct impact of the vertical motions on the evolution of sea ice signatures seen in the data, and to the first order the dominant role of horizontal motions could be assumed. As suggested by the reviewer, this issue is now briefly mentioned in the Conclusion section of the revised paper version.

"Moreover, the data are collected in September. This is related to the time of year of minimum sea ice extent and concentration. The summer sea ice melt is also nearing an end. Does this set up a shallow mixed layer regime in the MIZ that favors the presence of these mesoscale to submesoscale structures? If so, is there a seasonal variability to these SAR image expressions? It could be good to have this commented and/or addressed."

Thanks for pointing this. Yes, we agree that our observations made in mid-September might have some specific seasonal features, like the mentioned formation of the shallow mixed layer favorable for the generation of such dynamic features in the MIZ. Yes, we do expect that there is a certain seasonal variability of such SAR image expressions. This is confirmed, for example, by results of our recent SAR-based study in the Western Arctic Ocean, where analysis of the data from June to October showed a clear peak in the number of MIZ eddies in September-October of 2007, 2011 and 2016. Moreover, Bondevik (2011) in her Master thesis also showed that SAR-based detections of MIZ eddies along the East Greenland Current throughout the years of 2008 and 2009 had a distinct seasonal variability with

highest eddy numbers observed from May to September. In fact, we plan to address this question in more details for the Fram Strait MIZ in future by considering a longer time period of SAR observations. Some of the points mentioned above have been added to the revised paper version. Also, we had a reference to Bondevik (2011) work in our initial paper version, but due to the limit of 20 references we had to exclude it from the list. If the Reviewer feels it is necessary to have it, we will try to insert it at the expense of some other works.

"When Sentinel-1 is mentioned for the first time be more precise; e.g. Sentinel-1 is the European Radar Observatory for the Copernicus joint initiative of the European Commission (EC) and the European Space Agency (ESA)."

Thank you for the comment. We had no space to accommodate for this info in the abstract, yet, have given the full description in the main text when Sentinel-1 was first mentioned.

"Line 128/129: This sentence should be improved. Avoid expressions like…its movement direction…"

We have changed this to "…its propagation direction…", however, we don't know if this has improved the overall sounding of the sentence.

"Line 163: ··use same unit for EKE in text and Figure Maybe also color scale in the figure could be extended to identify values of 0.3 m^2/s^2".

Sorry, we couldn't get this as we have the same kinetic energy units expressed in the text and in the figure given in $m^2 s^{-2}$. Following your advice, we have adjusted the color scale to 0.25 m^2/s^2, as this gives a better visual expression as compared to the initial 0.2 m^2/s^2 and suggested 0.3 m^2/s^2.

Brief Communication: Mesoscale and submesoscale dynamics ~~of~~ in the marginal ice zone from sequential SAR observations

Igor E. Kozlov[1], Evgeny V. Plotnikov[1], Georgy E. Manucharyan[2]

[1]Remote Sensing ~~department~~Department, Marine Hydrophysical Institute of RAS, Sevastopol, 299011, Russia
[2]School of Oceanography, University of Washington, Seattle, 98195-7940, United States of America

Correspondence to: Igor E. Kozlov (igor.eko@gmail.com)

Abstract. New ~~possibility~~ possibilities for horizontal current retrieval ~~over~~ in ~~the~~ marginal ice zones (MIZs) from sequential Sentinel-1 synthetic aperture radar (SAR) images ~~is~~ are demonstrated. Daily overlapping SAR acquisitions ~~made~~ within 70-85° S/N ~~of latitude~~ at time intervals <1 hour enable ~~obtaining~~ estimation of high-resolution velocity fields, ~~and resolve~~ revealing MIZ dynamics down to submesoscales. An example taken from the Fram Strait MIZ reveals energetic ~~mesoscale and submesoscale~~ eddies and filaments with vorticities and divergences ~~horizontal velocities~~ normalized by the Coriolis parameter reaching O(1) magnitudes~~up to 0.75 m s^{-1}, strong sea ice convergence concentration and high vorticity values~~. The SAR-derived ~~Such~~velocity ~~observations~~ estimations at such high spatial resolution ~~are~~ can be critical for monitoring the evolving MIZ dynamics ~~in polar oceans as well as~~and model validation of submesoscale processes in polar oceans. ~~to and monitoring the current and future states of the marginal ice zones in the polar oceans.~~

1 Introduction

Marginal ice zones (MIZs) are regions of strong lateral buoyancy gradients, energetic atmosphere-ice-ocean interactions and enhanced biological productivity (~~refs?~~e.g. von Appen et al., 2018). With continuing global warming, MIZs remain a major source of uncertainties in sea ice prediction models (Tietsche et al., 2014) and their surface ~~area coverage~~extent ~~The width of the marginal ice zone (MIZ)~~ in the ~~polar~~ Arctic Ocean~~oceans~~ ~~is~~ ~~has~~ha~~ves~~ been~~rapidly~~ ~~growing~~ growing~~n~~ over the past several decades ~~over~~ during the past few decades (Strong and Rigor, 2013). ~~. While being a region of strong lateral buoyancy gradients, energetic atmosphere ice ocean interactions and enhanced biological productivity, the MIZ is also a major source of errors uncertainties in the long-term predictions of sea ice models (Tietsche et al., 2014).~~

MIZ dynamics and thermodynamics are critically affected by mesoscale and submesoscale eddies that are formed ~~exist in the MIZ interior and along the ice edge due to a~~due to a multitude of possible atmosphere-ice-ocean-~~ice~~ interaction mechanisms (e.g. Johannessen et al., 1987). Historical field campaigns have documented the presence of mesoscale eddy-related motions down to several hundred meters depth with associated mean orbital speeds of about 0.5 m s^{-1} in the Fram Strait MIZ (Wadhams and Squire, 1983; Johannessen et al., 1987). These ~~cyclonic~~ ice-edge eddies were observed to ~~not only swept~~mechanically sweep the ice away from the ice pack and to ~~, but also~~ entrain~~ed~~ the warm Atlantic Water (AW) beneath

Formatted: Not Highlight
Formatted: Not Highlight

the ice, causing an average ice edge ~~melt~~ retreat at a rate of 1-2 km day^{-1} in the summer (Johannessen et al., 1987). The ~~e~~Eddies ~~d~~dies have also contributed to a nonuniform ice motion leading to significant ice deformation, thus, enhancing the melting potential.

More recent model and field experiments also indicate ~~very~~ energetic motions associated with submesoscale eddies, fronts and filaments along the Arctic and Southern Ocean ~~the~~ MIZs (Manucharyan and Thompson, 2017; von Appen et al., 2018; Swart et al., 2020), which ~~that~~ importantly impact the heat and carbon exchange between the ocean and atmosphere. In particular, submesoscale ocean flows induce large vertical velocities that can ~~advect~~ entrain nutrients and relatively warm subsurface waters into the mixed layer with net vertical heat fluxes toward the ice surface reaching 100 W m^{-2} (Manucharyan and Thompson, 2017). They also lead to enhanced mixing of water masses over short horizontal scales, importantly shaping the sea ice and biology structure within the MIZ (von Appen et al., 2018).

Surface signatures of MIZ eddies and filaments can be effectively traced in high-resolution synthetic aperture radar (SAR) images due to characteristic patterns formed by sea ice that mimics the ocean current structure beneath (Shuchman et al., 1987; Kozlov et al., 2019). The manifestation of MIZ dynamics in SAR images is caused by the different level of radar backscatter from open water and low-concentration sea ice that tend to accumulate along the surface current convergence zones at eddy boundaries. Unlike the surfactant films that ~~marking~~ outline the eddy boundaries primarily under low winds (e.g. Karimova ~~&~~ and Gade, 2016), SAR signatures of sea ice are well sustained even under high wind conditions (Johannessen et al., 1987), providing almost all-weather capability for monitoring MIZ dynamics. In regions with relatively low ice concentrations (<50%), the sea ice tends to accumulate~~es~~ in predominantly cyclonic eddies and filaments, and the sea ice velocity becomes close to that of the surface ocean currents (Manucharyan & Thompson 2017), allowing one to make inferences about the upper ocean eddy dynamics from satellite sea ice observations.

Attempts to use spaceborne SAR data to retrieve sea ice motion in the polar oceans have been made since the launch of Seasat in 1978 (e.g. Hall and Rothrock, 1981), but relatively long sensing intervals (> 3 days) allowed to retrieve sea ice motions at relatively large scales, O(50-100 km). Having optimum capabilities to observe polar regions independent~~tly on~~ of illumination and weather conditions, the high-resolution SAR measurements are capable to resolve MIZ dynamics at significantly smaller scales, O(0.1-1 km), provided the time delay between sequential SAR images is sufficiently small, e.g. within 1-2 hours. However, until recently, such a combination was not realized in practice for non-commercial SAR missions.

The aim of this letter is to demonstrate a new possibility for regular SAR observations over the large MIZ regions that has recently ~~became~~ become available from sequential measurements of ~~Sentinel-1~~the European Radar Observatory for the Copernicus joint initiative of the European Commission (EC) and the European Space Agency (ESA) ~~(hereinafter, S-1)~~ Sentinel-1 A and B SAR missions launched in 2014 and 2016, respectively. As will be shown below, these data ~~enable~~ allows retrieving ~~to retrieve~~ the high-resolution sea ice velocity field ~~on a daily basis and~~ to observe the MIZ dynamics down to submesoscales on a daily basis. We believe that this information is critical for better understanding of the key dynamical

Formatted: English (U.S.)

Formatted: English (U.S.)

processes governing the submesoscale variability in MIZs, as well as for improving and validation of sea ice and coupled ice-ocean models.

2 Data and methods

Since the launch of the Sentinel-1B satellite in 2016, the SAR data from the two European polar-orbit Sentinel-1A and ~~S~~Sentinel-1B missions have become available for the public access. Each Sentinel-1 satellite carries a C-band SAR instrument operating at multiple sensing modes, each having a certain spatial resolution, a range of incidence angles, and a set of polarization channels.

Due to their polar orbits, Sentinel-1 A and B have high measurement frequency over the high-latitude regions. Many of the Sentinel-1 images overlap within the latitude band 70-85° in the southern and northern hemispheres, forming a distinct set of sequential SAR observations with a time lag of just around 50 minutes. As a result, ~~from~~ 2 to 4 overlapping scenes ~~are~~ can be available on a daily basis over certain regions~~the particular region of particular interest~~, ~~for example~~such as ~~over~~ the ~~Eurasian~~ European Arctic Ocean (Fig. 1, a). Fig. 1 (a) shows a map of the ~~western~~ European ~~Eurasian~~ Arctic with ~~locations of~~ 43 Sentinel-1 A/B ~~images~~ acquisitions available on 17 September 2017 at the Copernicus Open Access Hub (https://scihub.copernicus.eu). As is clearly seen, significant portions of the region, increasing northward, are covered by overlapping SAR ~~data~~scenes. The ~~Relatively~~ relatively short time lag between consecutive measurements, O(1 h), and the high spatial resolution of SAR data, O(100 m), ~~open up~~~~ensure~~provide a unique opportunity to observe the MIZ dynamics on the daily basis.

~~To illustrate demonstrate the potential of the data, here we~~We analyze Sentinel-1 SAR images acquired in September 2017 over Fram Strait (FS) (green frame in Fig. 1, a), the region of quasi-permanent ice edge formed between the warm Atlantic Water (AW) flowing northward into the Arctic Ocean and cold ice-covered Polar Water (PW) flowing southward (von Appen et al., 2016). It should be noted that our study period corresponds to the end of the melt season during which the formation of a shallow mixed layer in the MIZ might favor the presence of various mesoscale and submesoscale dynamic features. Though there might be a certain seasonal variability of such dynamic features seen in SAR data (e.g. Kozlov et al., 2019), this is not addressed here. The Copernicus Hub shows 120 SAR images available over FS in September 2017, ~~with~~ about half of which are ~~of them~~ forming pairs of partly overlapping sequential images. ~~In this work~~ Here we focus on a pair of Sentinel-1 images acquired on September 17, 2017 at 07:12 UTC (Sentinel-1A) and at 8:00 UTC (Sentinel-1B) with a time lag of 48 minutes (Fig. 1, b). The data are gridded Level 1 Extra-Wide swath mode medium-resolution (~90 m) products covering an area of ~400×400 km at HH and HV polarisations. The ~~Dual~~dual-polarized HH-band is further used for processing and analysis.

To estimate the velocity field ~~associated with~~from a pair of sequential SAR images, we implement the ~~The~~ following procedure ~~of velocity estimation from sequential SAR images has several main steps~~: i) image calibration for every image in the pair, ii) selection of overlapping image fragments, their normalization and filtering, iii) calculation of horizontal velocity

field for image fragments using one of the methods for velocity estimation from image sequences (e.g. Emery et al., 1986; Chen, 2011; Marmorino and Chen, 2019). ~~At first,~~The Sentinel-1 images ~~were~~ are calibrated to obtain the normalized radar cross-~~-~~section units. ~~Further, t~~The overlapping fragments of both images in the pair ~~were~~ are normalized to remove the signal trend in the range direction, and finally smoothed to reduce the speckle noise using the adaptive Wiener filter. The major issue arising at this step is the change in the SAR viewing geometry between sequential images. As a result, the level of radar backscatter over the particular surface area would differ from image to image, and so would affect the clarity of eddy manifestation in SAR images. This issue is addressed during the normalization step, but might be difficult to overcome for very thin ice whose backscatter is very sensitive to the described changes in the viewing geometry and near-surface winds. For demonstration, here we use the~~a~~ maximum cross-correlation method (MCC) (Emery et al., 1986; Qazi et al., 2014) to retrieve the surface velocity vectors, but we acknowledge that more elaborated velocit~~y~~metry methods can also be used for this purpose (see e.g. Chen, 2011; Marmorino and Chen, 2019)~~ over the MIZ~~. The preliminary analysis of SAR data from various dates in summer 2017 suggests that MCC works rather effectively for typical sea ice concentrations encountered along the ice edge and in the marginal ice zone, provided the movement of ice floes is apparent in the sequential SAR images. The MCC method was used with a moving window from 25×25 pixels for the initial large overlaps and down to 3×3 pixels for zooms over small-scale features with maximum allowed shifts up to 25 pixels in the zonal and meridional directions. For the pixel size of 40 m, the resulting velocity fields were obtained at 1 km and ~100 m resolution, respectively. ~~We also acknowledge that more elaborated alternative methods can be used for this purpose (see e.g. Chen, 2011; Marmorino and Chen, 2019).~~ Given the spatial resolution of the SAR images of 88×87 m in range and azimuth directions, pixel spacing of 40 m, and the time lag between sequential images equal to 48 minutes, the velocity detection threshold in this case would be 0.03 m s^{-1}~~;~~ ± 0.01 m s^{-1}~~-~~, similar to (Marmorino and Chen, 2019).

3 Results

3.1 Structure of MIZ

The positions of the two sequential Sentinel-1 SAR images acquired on September 17, 2017 over Fram Strait are shown in Fig. 1 (b). The area of the FS MIZ estimated directly from the SAR images is equal to ~~11~~15 000 km^2 with an average width of 60-70 km.~~,~~ The region ~~and possess display~~ contains a large number of small-to-mesoscale eddies, filaments and meanders, with some eddies appearing in the form of cyclone-anticyclone dipoles that are expected to form via instability of outcropping fronts (Manucharyan and Timmermans, 2013).~~.~~ Figure 1 (c) shows an enlarged fragment of the Sentinel-1A image ~~which~~ that clearly shows the manifestation of an anomalously large anticyclonic vortex (marked as **A** in Fig. 1, c) with a diameter of about 80-90 km spreading southward out of the main MIZ over the depths of around 2000 m. One can clearly see the formation of another smaller cyclonic vortex **C1** with a diameter of about 15 km on the western periphery of **A**. Many other small-scale eddies and meanders O(1 km) are seen along its periphery (Fig. 1, c). Notably, the periphery of the anticyclone **A** is bounded by several curved ice-filled narrow filaments, while a lot of open water with dispersed low-

concentration ice fields is found in the center. This is opposite for the cyclonic eddies **C1** and **C2** with more ice accumulated in their centers, in agreement with modeling studies demonstrating the preferential ~~results~~sea ice accumulation in cyclones (~~of~~ Manucharyan and Thompson, ~~(~~2017).

3.2 Velocity retrieval over MIZ

A fragment of the SAR image presented in Fig. 1 (c) was further used for surface current ~~retrieval~~ estimation using the MCC method. According to the WindSat and the ASCAT scatterometer~~s'~~ data for 17 September 2017 (not shown), the ~~near-surface~~ wind ~~field~~ conditions ~~was~~ were characterized by low south-easterly winds of 3-5 m s^{-1}~~, ., meaning that~~under which the ice drift near the ice edge should reflect the underlying ocean circulation (Shuchman et al., 1987; Manucharyan and Thompson, 2017).

Fig. 2 (a) shows the resulting velocity field obtained for the initial image fragment with the large anticyclonic vortex **A**. The overall geometry of the obtained current field is in a good agreement with the ice structures seen in the SAR image, and shows a pronounced anticyclonic rotation associated with the large vortex **A**. The modulus of horizontal current velocity $|\boldsymbol{u}|$, comprised of the eastward u and the northward v velocity components, is shown in Figure 2 (b). As seen, a general southeastward drift of the MIZ with an average velocity of 0.2-0.3 m s^{-1} is seen in the upper part of the image. It increases in the middle of the scene and forms a strong southward jet with current velocities reaching 0.75 m s^{-1}. This jet-like structure then evolves into the large ~~anticyclone~~ anticyclonic eddy **A** downstream. The mean orbital velocity of vortex **A** is about 0.4-0.5 m s^{-1}. However, the maximum values attain 0.65-0.75 m s^{-1} along its north-western periphery and 0.5 m s^{-1} along its southern boundary, gradually decreasing toward the center (Fig. 2, b). Such high velocity values are confirmed by the manual analysis of horizontal shifts of individual ice floes in sequential images (not shown).

Fig. 3 (a) shows the velocity field for the enlarged SAR fragment over the western part of the anticyclone **A**. A number of distinct dynamic features ~~is~~ are seen along its periphery, including the cyclonic vortex **C1** and the narrow elongated filaments **F1** and **F2**. As seen from Fig. 3 (a), all these features are well manifested in the SAR image due to enhanced radar backscatter from sea ice. The ~~latter~~ sea ice in the narrow filaments is likely accumulated ~~within narrow~~due to surface current convergence zones associated with ageostrophic secondary circulation near submesoscale fronts and filaments (McWilliams, 2016). The field of horizontal divergence, $\nabla \cdot \boldsymbol{u} = \partial u/\partial x + \partial v/\partial y$, confirms the formation of strong convergence zones up to -5×10^{-4} s^{-1} (blue color in Fig. 3, b) that correspond to bright sea ice patterns seen in the SAR image (Fig. 3, a). Thus, the presence of filamentary sea ice patterns is associated with regions of strong surface convergence and downwelling.

As noted above, the periphery of the anticyclone **A** is bounded by several narrow filaments (Fig. 3, a). Filament **F1** is 0.5-1.5 km wide and ~60 km long, very similar to the submesoscale cyclonic filament sampled in detail in the Fram Strait MIZ by von Appen et al. (2018) where velocities of ±0.5 m s^{-1} were observed with a vessel mounted acoustic Doppler current profiler. However, as both the interpretation of the SAR image and the retrieved current velocity suggest, this filament is not a stand-alone feature, but is a part of the larger eddy-induced frontogenesis pattern and, hence, cannot be interpreted out of

the context. The important consequence is that its ~~movement~~ propagation direction and, hence, the sign of relative vorticity, $\zeta = \partial v/\partial x - \partial u/\partial y$, is different depending on its part to be considered (Fig. 3, c).

The data show that **F1** is stretching along-front in~~to the~~ opposite directions and moves northward with a mean (maximum) speed of 0.4-0.5 (0.75) m s^{-1} in its upper half, while drifting southward at an average (maximum) velocity of 0.3-0.4 (0.55) m s^{-1} in the lower part, as shown by arrows in Fig. 3 (a). The cross-front velocity is almost negligible in its southern and northern parts, while it attains ~0.05-0.1 m/s near the divergence point (found next to **F1** notion in Fig. 3, a). The relative vorticity ζ values estimated for the mean current velocity $\Delta v = 0.4$ m s^{-1} and characteristic filament cross-front width $\Delta x =$ 1 km are $\zeta = \Delta v/\Delta x = \sim 3f$, where f is the Coriolis parameter equal $f = 1.433 \cdot 10^{-4} s^{-1}$ for latitude $\theta = 80.2°$ N. This gives the Rossby number $Ro = \zeta/f \sim O(1)$, clearly indicating the~~a~~ submesoscale nature of this filament. Similar stretching and movement into the opposite directions are ~~also~~ observed for the filament **F2**, which also splits into the cyclonic and anticyclonic counterparts (Fig. 3, c). Its cyclonic part starts to meander and then rotates anticlockwise to shape the boundary of the cyclone **C1**.

The shape of the cyclone **C1**, defined from the orientation of the bounding ice streaks, is highly elliptical with the minor and major axis being about 10 km ~~and major – about~~and 25 km, respectively (Fig. 3, a). The associated orbital velocities are 0.2-0.65 m s^{-1} (mean value 0.5 m s^{-1}), being largest along its major axis on the western and eastern sides, and smallest near the eddy center. The horizontal divergence field shows high negative values (convergence) where sea ice accumulates along the eddy boundaries (compare Figs. 3a and 3b). As noted above, the ice concentration at the boundaries and in the center of **C1** is higher than for eddy **A**. This is confirmed by the more intense surface convergence over **C1** (Fig. 3, b) that is presumably linked to stronger ageostrophic motions. Indeed, the comparison of vorticity values for eddies **A** ($\zeta \approx 0.07f$) and **C1** ($\zeta \approx 0.3f$) ~~shows~~ yields a ~~higher~~ larger Rossby number than for the cyclone **C1** with ageostrophic effects playing a higher role in this case.

Fig. 3 (d) shows the field of instantaneous kinetic energy (KE), $KE = \frac{1}{2}(u^2 + v^2)$. In general, one ~~may~~ sees ~~a~~ very energetic patterns associated with eddy dynamics in the MIZ with the mean KE of about 0.1 $m^2 s^{-2}$. ~~As seen, the~~ and the maximum of ~~the KE reaches~~ 0.23 $m^2 s^{-2}$ over the northern periphery of **A** ~~with the mean value of about 0.1 $m^2 s^{-2}$~~. For the cyclone **C1**, ~~it~~ the KE is slightly less, but still high~~.~~ ~~:~~ ~~The~~ the maximum value of 0.2 $m^2 s^{-2}$ is found over the western periphery of **C1**, while over the eastern part it is about 0.1-0.15 $m^2 s^{-2}$.

4 Discussion and conclusions

~~In this letter w~~We demonstrated a new possibility to retrieve horizontal velocity fields from ~~–~~ sequential Sentinel-1 SAR images taken over low-concentration ice regions ~~of polar oceans~~ where sea ice motion is indicative of mesoscale and submesoscale eddies and filaments. The pair of Sentinel-1 SAR images acquired over the Fram Strait MIZ revealeds a large anticyclonic ice-edge eddy of 80-90 km in diameter and numerous cyclonic eddies of smaller size at its periphery, bounded by several elongated ice-filled filaments. The reconstructed currents ~~show that maximum orbital velocities of the large~~

~~anticyclone exceed 0.7 m s^{-1}~~revealed strong convergence zones and relative vorticity magnitudes corresponding to O(1) Rossby numbers. While historic field campaigns have documented the generation of ice-edge eddies in central Fram Strait (e.g. Wadhams and Squire, 1983; Johannessen et al., 1987; Shuchman et al., 1987), the observations of such an anomalously large and energetic MIZ eddy in the Arctic Ocean have never been reported before.

Notably, the location of MIZ eddies reported here coincides with the ice edge region in central FS characterized by high summer-time eddy kinetic energy (EKE) values (exceeding 0.02~~00~~ ~~e~~m^{-2} s^{-2}) reported by Bulczak et al. (2014) based on satellite altimetry data, and later confirmed by long-term mooring observations (von Appen et al., 2016). Such anomalously high EKE values ~~relative to adjacent regions~~ were attributed to the complex atmosphere-ice-ocean interplay, including the formation of eddies due to barotropic and baroclinic instability of an ice edge jet along the MIZ, topographic generation and trapping, interaction of AW eddies advected to the ice edge with meltwater fronts, wind-induced differential Ekman pumping along a meandering ice edge, or their combinations (Johannessen et al., 1987). The lifetime of such eddies was reported to be at least 20-30 days with diameters ranging within 20-40 km, rarely reaching 60 km (Wadhams and Squire, 1983). In our case, surface signatures of the large anticyclone were clearly seen only for about 10 days from 14 September until 24 September 2017, when it became fully ice-filled and indiscernible from the main MIZ region.

The SAR data also reveals the development of several elongated filaments and smaller-scale cyclones on the periphery of the large anticyclone. The latter is frequently reported in literature (e.g. Zatsepin et al., 2019) and is attributed to horizontal shear instabilitie~~s~~y of anticyclonic flows that are very effective int~~o~~ producing~~e~~ submesoscale cyclones (McWilliams, 2016). The ~~Analysis~~ analysis of the reconstructed current velocity and the filament length~~-~~scale clearly shows submesoscale nature of these features with ~~vertical~~ relative vorticity being about three times the Coriolis frequency. Similarly, strong filaments were recently reported by von Appen et al. (2018) based on detailed field observations in the central FS, showing that in regions where AW and PW meet such filaments could be deep reaching with substantial vertical motions and density anomaly extending down to 400 m depth, potentially influencing biomass and nutrient distributions in the water column. Such submesoscale processes, as well as wind-induced upwelling in the MIZ, are often associated with intense vertical motions that, in turn, might influence the evolution of the sea ice patterns observed in the SAR data. However, as the time gap between sequential SAR images is < 1 hour, the effect of vertical motions with typical velocities around 0.001-0.01 m s^{-1} (e.g. von Appen et al., 2018) will be negligibly small at such time scales.

As revealed from the SAR data, these elongated filaments move at the maximum speed of 0.75 m s^{-1}, being a part of the larger eddy-induced frontogenesis pattern. They are stretching and moving in~~to the~~ opposite directions, delineating a dipole eddy structure with opposite vorticity sign. Due to their large spatial extent in the along-front direction, such peculiarities of the submesoscale flow could be hardly resolved even in specialized high-resolution field observations~~, when a different velocity structure would be inferred *in situ* depending on the measurement location relative to the filament part~~ because of their limited spatial coverage. The latter clearly emphasizes the ~~capability~~ advantage of high-resolution sequential SAR data ~~to~~ in resolvinge small-scale MIZ ~~peculiarities~~ processes ~~of the complex MIZ dynamics~~. Given the abundance of MIZ eddies and fronts in the Arctic and Southern Oceans (Kozlov et al., 2019; Swart et al., 2020; von Appen et al., 2018), these

energetic features may importantly ~~influence~~ enhance the vertical heat transport toward the sea ice and influence sea ice melt, upper ocean stratification, and distribution of nutrients and buoyant materials in the water column.

Apart from its potential use in validation and improvement of sea ice forecasting models, the availability of daily, regular, and high-resolution sequential Sentinel-1 SAR observations could contribute to guiding field campaigns and advancing our understanding of multi-scale atmosphere-ice-ocean interactions in ~~the marginal ice zones~~MIZs, identifying hot-spots of high kinetic energy, and quantifying lateral and vertical dispersion of various buoyant materials, including microplastics and oil pollution in the polar oceans.

Acknowledgments

This study was supported by Russian Science Foundation grant No. 18-77-00082. Software development for data analysis was partly made under the Ministry of Science and Higher Education of the Russian Federation contract no. 0827-2020-0002~~.~~. G.E.M. acknowledges support from the United States National Science Foundation, Grant No. 1829969. Sentinel-1 SAR data used in this study can be freely accessed from Copernicus Open Access Hub at https://scihub.copernicus.eu. The authors declare that they have no conflict of interest.

References

Bulczak, A. I., Bacon, S., Naveira Garabato, A. C., Ridout, A., Sonnewald, M. J., and Laxon, S. W.: Seasonal variability of sea surface height in the coastal waters and deep basins of the Nordic Seas, Geophys. Res. Lett., 42, 113–120, https://doi.org/10.1002/2014GL061796, 2015.

Chen, W.: Nonlinear inverse model for velocity estimation from an image sequence, J. Geophys. Res., 116 (06015), https://doi.org/10.1029/2010JC006924, 2011.

Emery, W. J., Thomas, A. C., Collins, M. J., Crawford, W. R., and Mackas, D. L.: An objective method for computing advective surface velocities from sequential infrared satellite images, J. Geophys. Res., 91(C11), 12865–12878, https://doi.org/10.1029/JC091iC11p12865, 1986.

Hall, R. T., and Rothrock, D. A.: Sea ice displacement from Seasat synthetic aperture radar, J. Geophys. Res., 86(C11), 11078–11082, https://doi.org/10.1029/JC086iC11p11078, 1981.

Johannessen, J. A., Johannessen, O. M., Svendsen, E., Shuchman, R., Manley, T., Campbell, W. J., Josberger, E. G., Sandven, S., Gascard, J. C., Olaussen, T., Davidson, K., and Van Leer, J.: Mesoscale eddies in the Fram Strait marginal ice zone during the 1983 and 1984 Marginal Ice Zone Experiments, J. Geophys. Res.: Oceans, 92(C7), 6754-6772, https://doi.org/10.1029/JC092iC07p06754, 1987.

Karimova, S. and Gade, M.: Improved statistics of sub-mesoscale eddies in the Baltic Sea retrieved from SAR imagery, Int. J. Remote Sens, 37, 2394–2414, https://doi.org/10.1080/01431161.2016.1145367, 2016.

Kozlov, I. E., Artamonova, A. V., Manucharyan, G. E., and Kubryakov, A. A.: Eddies in the Western Arctic Ocean from spaceborne SAR observations over open ocean and marginal ice zones, J. Geophys. Res.: Oceans, 124(9), 6601-6616, https://doi.org/10.1029/2019JC015113, 2019.

Manucharyan, G. E. and Thompson, A. F.: Submesoscale sea ice–ocean interactions in marginal ice zones, J. Geophys. Res.: Oceans, 122(12), 9455-9475, https://doi.org/10.1002/2017JC012895, 2017.

Marmorino, G., and Chen, W.: Use of WorldView-2 Along-Track Stereo Imagery to Probe a Baltic Sea Algal Spiral, Remote Sens., 11(7), 865, https://doi.org/10.3390/rs11070865, 2019.

Manucharyan, G. E. and Timmermans, M. L.: Generation and separation of mesoscale eddies from surface ocean fronts, J. Phys. Oceanogr., 43(12), 2545-2562, https://doi.org/10.1175/JPO-D-13-094.1, 2013.

McWilliams, J. C.: Submesoscale currents in the ocean, Proc. Royal Soc. A. 472 (2189). https://doi.org/10.1098/rspa.2016.0117, 2016.

~~Mensa, J. A., Timmermans, M. L., Kozlov, I. E., Williams, W. J., and Özgökmen, T.: Surface drifter observations from the Arctic Ocean's Beaufort Sea: Evidence for submesoscale dynamics. J. Geophys. Res.: Oceans, 122(12), 9455–9475, https://doi.org/10.1002/2017JC013728, 2018.~~

Qazi, W. A., Emery, W. J., and Fox-Kemper, B.: Computing ocean surface currents over the coastal California current system using 30-min-lag sequential SAR images, IEEE Trans. Geosci. Rem. Sens., 52, 7559–7580, doi:10.1109/TGRS.2014.2314117, 2014.

Shuchman, R. A., Johannessen, O. M., Campbell, W. J., Lannelongue, N., Burns, B. A, Josberger, E. G., and Manley, T.: Remote sensing of the Fram Strait marginal ice zone. Science, 236, 427–439. https://doi.org/10.1126/science.236.4800.429, 1987.

Strong, C., and Rigor, I. G., Arctic marginal ice zone trending wider in summer and narrower in winter, Geophys. Res. Lett., 40, 4864– 4868, https://doi.org/10.1002/grl.50928, 2013.

Swart, S., du Plessis, M. D., Thompson, A. F., Biddle, L. C., Giddy, I., Linders, T., Mohrmann, M. and Nicholson, S. A.: Submesoscale fronts in the Antarctic marginal ice zone and their response to wind forcing, Geophys. Res. Lett., 47, e2019GL086649, https://doi.org/10.1029/2019GL086649, 2020.

Tietsche, S., Day, J. J., Guemas, V., Hurlin, W. J., Keeley, S. P. E., Matei, D., Msadek, R., Collins, M. and Hawkins, E.: Seasonal to interannual Arctic sea ice predictability in current global climate models. Geophys. Res. Lett., 41, 1035–1043. https://doi.org/10.1002/2013GL058755, 2014.

von Appen, W. J. V., Schauer, U., Hattermann, T., and Beszczynska-Möller, A.: Seasonal cycle of mesoscale instability of the West Spitsbergen Current, J. Phys. Oceanogr., 46(4), 1231-1254, https://doi.org/10.1175/JPO-D-15-0184.1, 2016.

von Appen, W. J., Wekerle, C., Hehemann, L., Schourup-Kristensen, V., Konrad, C., and Iversen, M. H.: Observations of a submesoscale cyclonic filament in the marginal ice zone. Geophys. Res. Lett., 45(12), 6141-6149, https://doi.org/10.1029/2018GL077897, 2018.

Formatted: Font: Not Italic

Formatted: Font: Not Italic

Formatted: Font: Not Italic

Formatted: Font: Not Italic

Wadhams P., Squire V. A., An ice-water vortex at the edge of the East Greenland Current, J. Geophys. Res., 88(C5), 2770–2780, https://doi.org/10.1029/JC088iC05p02770, 1983.

Zatsepin, A., Kubryakov, A., Aleskerova, A., Elkin, D. and Kukleva, O.: Physical mechanisms of submesoscale eddies generation: evidences from laboratory modeling and satellite data in the Black Sea. Ocean Dyn. 69, 253–266, https://doi.org/10.1007/s10236-018-1239-4, 2019.

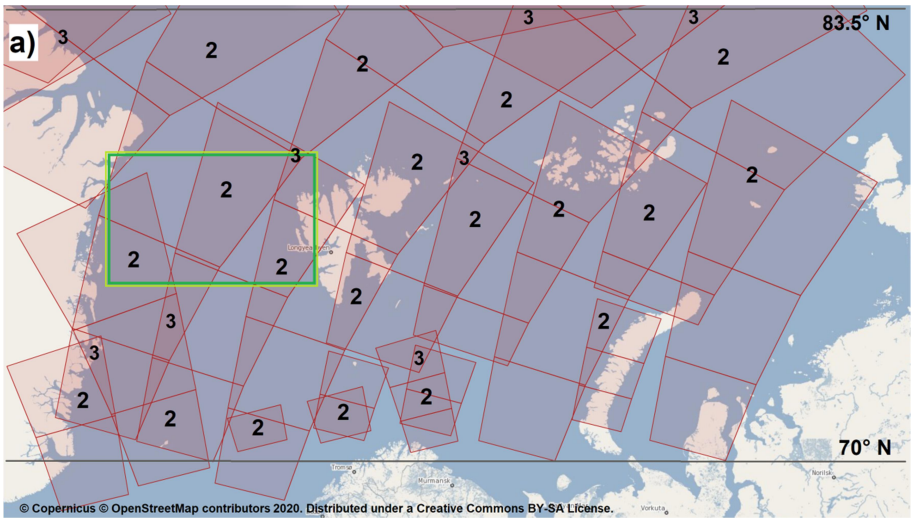

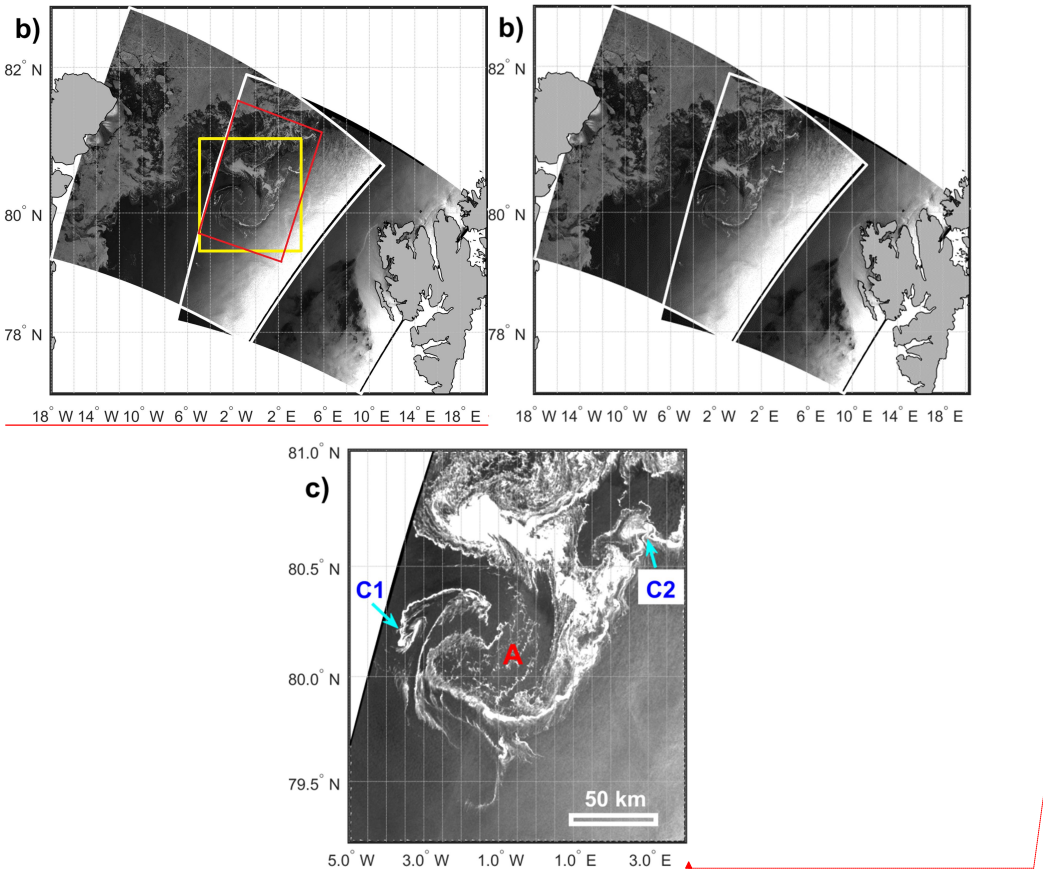

Formatted: English (U.S.)

Figure 1: a) Map of the ~~western Eurasian~~ Europian Arctic showing the ~~acquisition~~ coverage ~~tracks~~ of Sentinel-1 A/B SAR image acquisitions~~s~~ available on 17 September 2017. Pink frames mark the borders of individual SAR images, while digits show the number of overlapping SAR frames. Grey lines mark latitude boundaries of 70° N and 83.5° N. Green box shows the area of Fram Strait. The map is taken from Copernicus Open Access Hub © Copernicus © OpenStreetMap 2020. Distributed under a Creative Commons BY-SA License. b) Position of two sequential Sentinel-1 A/B images acquired on September 17, 2017 over Fram Strait. Red and yellow frames mark the regions enlarged in c) and in Figure 2 (a). c) Enlarged fragment of Sentinel-1A image for the same date (07:12 UTC) with distinct signatures of a large anticyclone and several cyclones in the marginal ice zone. Letters A, C1, C2 mark eddies described in the text.

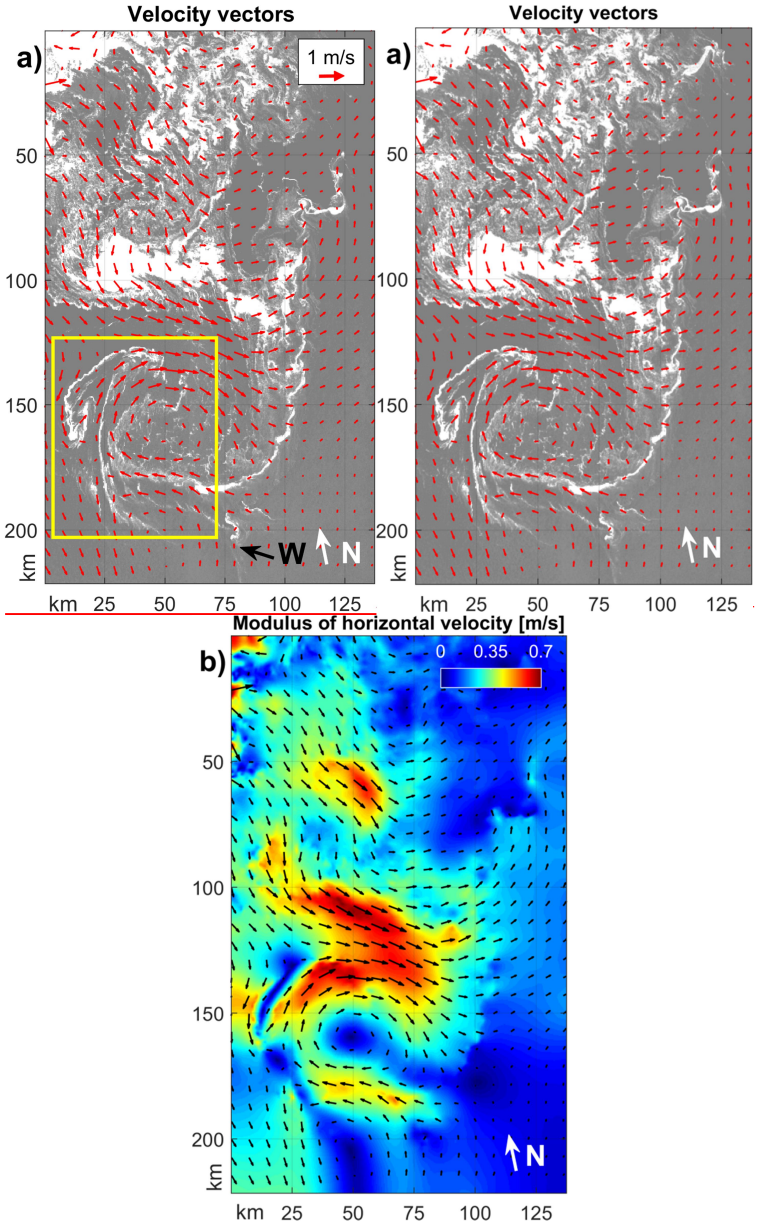
Velocity vectors
a)
1 m/s
50
100
150
200
km
W
N
km 25 50 75 100 125
Velocity vectors
a)
50
100
150
200
km
N
km 25 50 75 100 125
Modulus of horizontal velocity [m/s]
b)
0 0.35 0.7
50
100
150
200
km
N
km 25 50 75 100 125

Figure 2: The horizontal velocity vectors calculated from two sequential Sentinel-1 A/B images ~~taken~~ acquired on September 17, 2017 over Fram Strait using the MCC method superimposed on a) the SAR image and b) map of the ~~modulus of the~~ horizontal velocity (speed in color). Letters W and N mark the wind and the northern directions. Yellow frame in (a) shows the region enlarged in Figure 3.

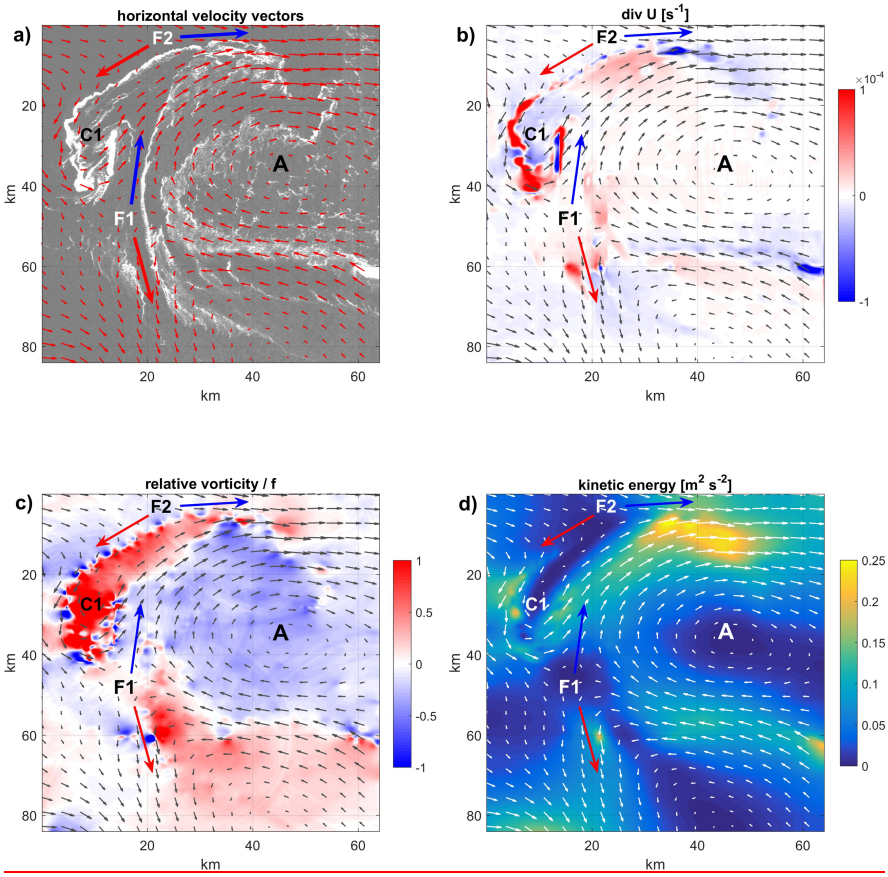
a)
horizontal velocity vectors
F2
C1
A
F1
km
20
40
60
80
b)
div U [s-1]
×10-4
1
0
-1
c)
relative vorticity / f
0.5
-0.5
d)
kinetic energy [m2 s-2]
0.25
0.2
0.15
0.1
0.05

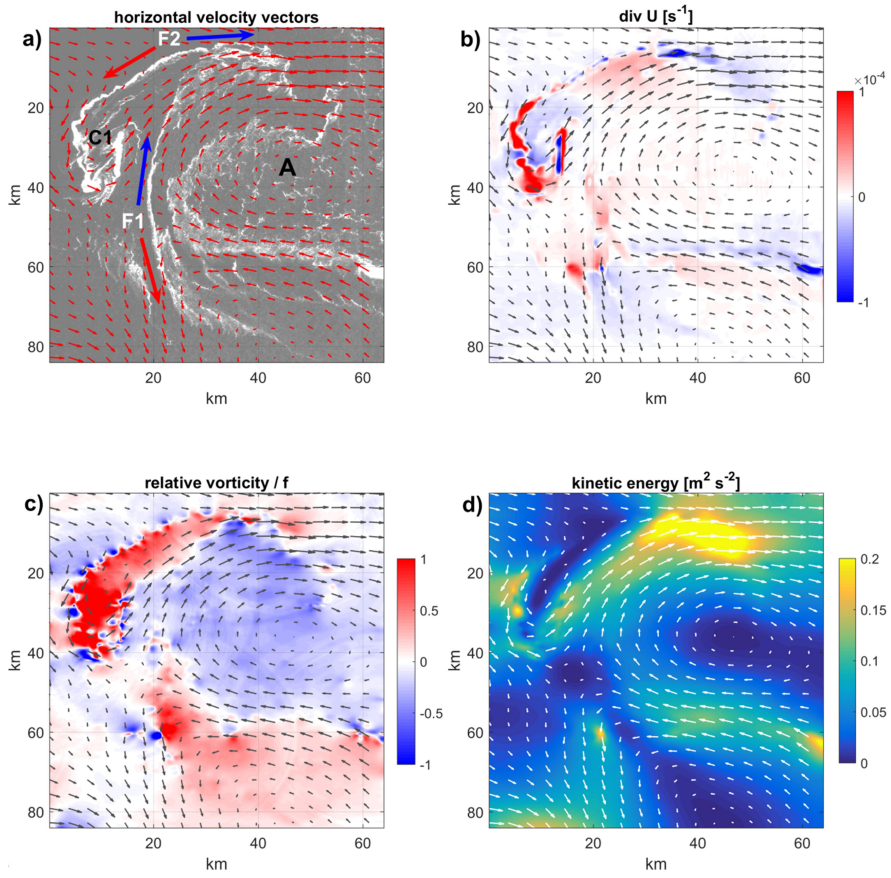

Figure 3: Results for zoomed area over anticyclone A and cyclone C1: (a) horizontal velocity vectors; (b) horizontal divergence, (c) relative vorticity ~~divided~~ normalized by the Coriolis parameter; (d) kinetic energy. The largest vector in (a) has a magnitude of 0.75 m s^{-1}. Letters A, C1, F1 and F2 ~~in c)~~ mark the locations of the eddies and filaments described in the text, while blue and red arrows show the movement direction of the filaments F1 and F2.